[16] W. Li and M. Nasrabadi, "Object recognition based on graph matching implemented by a Hopfield-style neural network," *Int. J. Conf. Neural Networks*, Washington, DC, June 18–22, 1989, vol. 2, pp. 287–290.
[17] W. C. Lin, F. Liao, C. Tsao, and T. Lingutla, "A hierarchical multiple-view approach to three-dimensional object recognition," *IEEE Trans. Neural Networks*, vol. 2, pp. 84–92, Jan. 1991.

A Hough Transform for Detecting the Location and Orientation of Three-Dimensional Surfaces Via Color Encoded Spots

Colin J. Davies and Mark S. Nixon

***Abstract*—Video-rate three-dimensional (3-D) acquisition is desirable, in particular for capturing the mouth's shape when modeling the vocal tract. In a new structured light technique, scenes are illuminated by an array of circular spots which are color encoded to resolve spatial ambiguity. The position and shape of the imaged spots depend on the location and orientation of the illuminated 3-D surface. We present a novel 3-D Hough transform (HT) to detect 3-D surface location and orientation via the imaged spots, with voting constraints applied to maximize potential accuracy. This new technique is demonstrated to successfully extract the 3-D data for a moving face from images acquired at video-rate.**

I. Introduction

A desirable aid to enhance models of speech production is the capture of the dynamic three-dimensional (3-D) shape of the mouth during speech, as lip movement is important in speech production and perception [12]. A range of techniques have been developed to sense 3-D surface shape [1], but many techniques are restricted to static or slowly moving objects. Photometric stereo requires multisite illumination and hence multiple images, rendering it to be ill-suited for dynamic scene acquisition. One system [3], reconstructed 3-D head images by projecting pattern sequences; however, due to its sequence-basis, it cannot be deployed in speech applications. Video-rate triangulation based structured light systems enable 3-D surface data acquisition for dynamic scenes. The surface depth information is calculated from a single image of the scene, illuminated by a single projected pattern of structured light. Thus the data required to calculate the 3-D shape information can be captured at video-rate, although the processing required to calculate the dynamic 3-D shape information for the video sequence is performed off-line. Stripes [2], [10], [12], grids [6], and square-based pattern elements [9], [15], [16] have previously formed the basis of the projected patterns. In the approach presented here, the projected structured light pattern is an array of color encoded circular spots. Each imaged spot is deformed by the underlying surface, both in position and in shape. From the observed ellipses, the 3-D surface location and orientation can be captured simultaneously [4], [5].

In application, step edges in the illuminated surface can bisect projected pattern elements resulting in incomplete imaged shapes. For pattern elements based upon stripes or squares, incomplete imaged-shapes are not uniquely identifiable, admitting the possibility of erroneous depth measurements; a square projected onto an inclined surface may be imaged as a rectangle, regardless of the presence or absence of a step edge. When the pattern elements are circular spots, incomplete shapes are immediately apparent.

Manuscript received August 12, 1995; revised November 25, 1996.

C. J. Davies is with NDS Ltd., Chilworth, Hampshire SO16 7NS, U.K. (e-mail: cdavies@ndsuk.com).

M. S. Nixon is with the Image, Speech, and Intelligent Systems Research Group, Department of Electronics and Computer Science, University of Southampton SO17 1BJ, U.K. (e-mail: msn@ecs.soton.ac.uk)

Publisher Item Identifier S 1083-4419(98)00210-6.

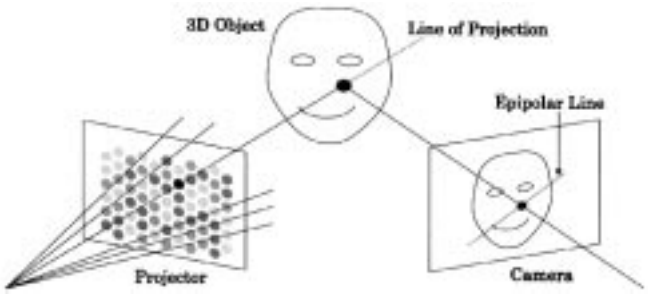

Fig. 1. The structured light system's geometry.

A priori knowledge can be used to increase the efficiency of feature extraction. In the new 3-D sensing system, the center position of each imaged spot is constrained to lie on an epipolar line, restricted by the working volume of the system. The imaged shape of each spot depends on the orientation of the illuminated surface. These constraints are applied in a novel formulation of the Hough transform (HT) to extract the imaged spots. The HT has an accumulator space of only three parameters that completely describe the 3-D surface's location and orientation.

Section II develops the relationship of each imaged spot's position and shape to the illuminated surface's location and orientation. In Section III, the formulation of the HT to extract the imaged spots is detailed. Section IV describes the implementation of the HT which includes voting constraints to reduce the number of background votes cast in the HT accumulator array to minimize the number of false peaks. Results in Section V verify the new formulation of the HT and demonstrate how this new structured light system can be used to recover 3-D surface shape for imagery acquired at video-rate.

II. Parameterizing the Imaged Spots

Fig. 1 shows a schematic of the structured light system's geometry. A projector illuminates the scene with a hexagonally tessellated array of color encoded circular spots, the scene is imaged by a camera offset from the projector. For each projected spot, a spatial codeword formed from the color of the spot and those of its immediate neighbors identifies the spot's position in the projected array. If the projector and camera are calibrated with respect to a known 3-D coordinate system then the center of each imaged spot is constrained to lie along a known epipolar line. From the imaged position of each spot's center, a sample of the surface location is determined using triangulation.

The shape of each imaged spot depends on the nature and orientation of the 3-D surface it illuminates. If the surface area illuminated by an individual spot is planar, the imaged spot will be perceived as an ellipse. Fig. 2 shows views of a circular spot projected onto the surface of a wedge. The projector and camera are horizontally aligned and perspective effects considered negligible. For this example, the epipolar line, along which the spot's center lies in the camera image, is horizontal. The imaged ellipse shape is observed to be the projected circle sheared and scaled in the direction of the epipolar line. Altering the orientation of the illuminated 3-D surface alters the observed

Fig. 2. Views of a spot projected onto the surface of a wedge (projector and camera horizontally aligned).

shear and scale, there is no change in the spot's height perpendicular to the epipolar line. These observations suggest that a suitable parameterization of the imaged spot's shape is the transformation of a circle by shear and scaling in the direction of the epipolar line, which is a parameterization related to the illuminated 3-D surface's orientation.

Using the matrix representation of an ellipse [8], the imaged ellipse shape is considered as an affine transformation of the unit diameter circle centered at the imaged ellipse center. The unit diameter circle centered at the origin is given by

$$\underline{\mathbf{u}}^T \underline{\mathbf{u}} = 1/4 \tag{1}$$

where $\underline{\mathbf{u}} = [x \quad y]^T$. Let x be the direction along and y the direction perpendicular to the spot center's epipolar line in the image.

For the imaged ellipse shape the affine transformation is restricted to shear and scaling in the direction of the epipolar line, with no translation vector. Defining a transformed coordinate space $\underline{\mathbf{v}} = [i \quad j]^T$

$$\underline{\mathbf{v}} = S\underline{\mathbf{u}} \tag{2}$$

where

$$S = \begin{bmatrix} \gamma & \tau \\ 0 & 1 \end{bmatrix}$$

such that γ is the scaling factor and τ is the shear in the direction of the spot center's epipolar line in the image.

By substitution in (1)

$$\underline{\mathbf{v}}^T [S^{-1}]^T S^{-1} \underline{\mathbf{v}} = 1/4 \tag{3}$$

where

$$[S^{-1}]^T S^{-1} = \begin{bmatrix} \frac{1}{\gamma^2} & \frac{-\tau}{\gamma^2} \\ \frac{-\tau}{\gamma^2} & 1 + \frac{\tau^2}{\gamma^2} \end{bmatrix}.$$

The imaged ellipse is then

$$[i \quad j] \begin{bmatrix} \frac{1}{\gamma^2} & \frac{-\tau}{\gamma^2} \\ \frac{-\tau}{\gamma^2} & 1 + \frac{\tau^2}{\gamma^2} \end{bmatrix} \begin{bmatrix} i \\ j \end{bmatrix} = 1/4. \tag{4}$$

The imaged spot's shape is related to the orientation of the illuminated surface. Let the surface orientation be defined by the angles in Fig. 3; In the epipolar plane, defined by the projected and imaged spot center rays, θ is the angle between the rays as calculated from the calibration data, ϕ is the angle of the projected ray to the surface. Relative to the normal of this plane, α is the surface orientation angle in the direction of the projected ray.

With respect to the epipolar plane let p be the width of the projected circle, s the width of the ellipse on the surface and c the width of the imaged ellipse, as shown in Fig. 4. For a constant angle θ, only by varying ϕ will c, the width of the imaged ellipse, alter. Forming the triangle to relate p and s

$$\sin\phi = \frac{p}{s} \tag{5}$$

so

$$s = \frac{p}{\sin\phi}. \tag{6}$$

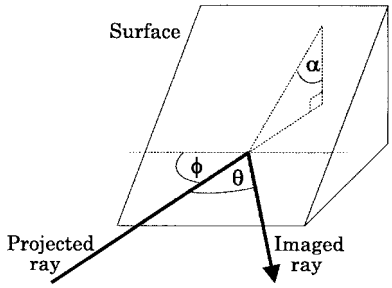

Fig. 3. Angles for the surface orientation problem.

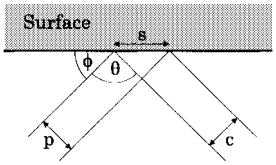

Fig. 4. Defining the projected, surface, and imaged spot widths in the epipolar plane.

For c and s

$$\sin(\pi - (\phi + \theta)) = \frac{c}{s} \tag{7}$$

so

$$s = \frac{c}{\sin\theta\,\cos\phi + \cos\theta\,\sin\phi}. \tag{8}$$

Combining (6) and (8)

$$\frac{c}{p} = \frac{\sin\theta\,\cos\phi + \cos\theta\,\sin\phi}{\sin\phi} = \frac{\sin\theta\,\cos\phi}{\sin\phi} + \cos\theta. \tag{9}$$

The ratio c/p is the scaling factor γ in the direction of the epipolar line from the ellipse matrix of (4)

$$\gamma = \frac{\sin\theta}{\tan\phi} + \cos\theta. \tag{10}$$

For a constant angle θ, between the projected and imaged rays, and for a constant surface angle ϕ, varying the surface orientation angle α shears the imaged ellipse in the direction of the epipolar line. To find the shear factor τ, we consider the solid plane geometry of Fig. 5. The imaged and projected rays form a horizontal plane, the angles are as defined in Fig. 3. The projection of a unit vertical length onto the inclined surface plane enables us to calculate the imaged shear. For the length a

$$a = \tan\alpha. \tag{11}$$

The triangle to find length b

$$b = a\sin\theta. \tag{12}$$

Since we considered the projection of a unit vertical length, b is the imaged shear factor from the ellipse matrix of (4)

$$\tau = \tan\alpha\,\sin\theta. \tag{13}$$

III. Formulation of the HT

If a conventional parameterization of the ellipse were to be applied to detect the imaged spots, a suitably formulated HT would require a five-dimensional HT accumulator which has large computational requirements. We have shown above, how for the new structured light system, each imaged spot may be described by only three parameters: the spot's center position along the epipolar line with shear and scale

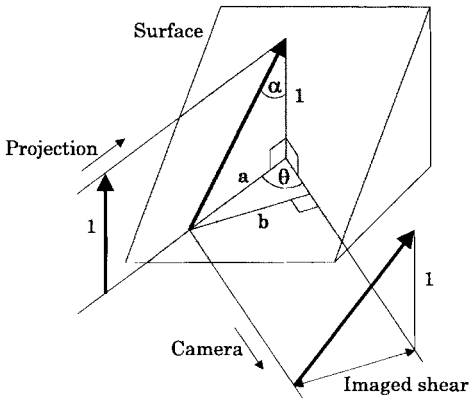

Fig. 5. Projection of a unit vertical length to determine the imaged shear.

parameters to describe its shape. From these parameters the 3-D location and orientation of the illuminated surface are calculated. These are the parameters of direct interest in 3-D imaging and the spots act as an intermediary in their detection. In this section a novel HT to extract each imaged spot is formulated based on only three parameters.

For a given spot and image edge point, all possible combinations of the three parameters are found which correspond to the edge point lying on the perimeter of the spot. Votes are cast for these parameter combinations in a 3-D accumulator array. Peaks in the array correspond to the maximum likelihood parameterizations of the imaged spot.

To parameterize the HT to extract the imaged spots the imaged ellipse shape matrix of (4) is used, which is of the quadratic form

$$[i \quad j]\begin{bmatrix} A & B \\ B & D \end{bmatrix}\begin{bmatrix} i \\ j \end{bmatrix} = 1/4. \tag{14}$$

The axes of the imaged ellipse matrix are aligned such that i and j are the direction along and perpendicular, respectively, to the spot center's epipolar line in the image. The i and j distances are normalized with respect to the known and fixed imaged spot size in the direction perpendicular to the epipolar line. For an edge point to lie upon the ellipse perimeter of a given spot, $|j| \leq 1/2$. The position of the edge point in the direction along the epipolar line axis is known.

For a given spot and considered edge point, votes are cast in the 3-D HT parameter space for the ellipse center positions along the epipolar line corresponding to possible combinations of the two ellipse shape parameters τ and γ. To find the center positions along the epipolar line (4) is solved for i, the normalized offset of the center from the position of the edge point along the epipolar line

$$i = \frac{\frac{8j\tau}{\gamma^2} \pm \sqrt{\frac{64j^2\tau^2}{\gamma^4} - \frac{16}{\gamma^2}\left(-1 + 4j^2\left(1 + \frac{\tau^2}{\gamma^2}\right)\right)}}{\frac{8}{\gamma^2}} \tag{15}$$

which simplifies to

$$i = j\tau \pm \gamma\sqrt{(1/4 - j^2)}. \tag{16}$$

Equation (16) shows that for each considered edge point of a given spot there are two planes of votes to be cast across the accumulator array, which is 3-D in terms of the possible values for the center position of the spot along its epipolar line and the two shape parameters τ and γ. The reason for there being two planes is clearly seen when we consider edge point A of Fig. 6. For given values for τ and γ, there are two possible ellipses centered on the epipolar line for which edge point A lies on the perimeter.

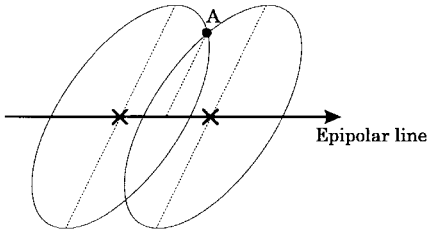

Fig. 6. The possible ellipses for a single edge point and surface orientation which are centered on the epipolar line.

IV. Implementation of the HT

A. Resolution of the HT Accumulator Array

The 3-D parameter space of the HT is represented in discrete form by the 3-D HT accumulator array. For accurate parameter extraction it is desirable to use a fine resolution HT accumulator array. However, the resolution of the HT accumulator array must be such that a single peak occurs in a single accumulator cell for a given imaged spot. If the peak spreads to adjacent accumulator cells then the resolution is too fine [11], [14].

In the formulation of the HT to extract the imaged spots a natural progression is to substitute (10) and (13) for τ and γ in (16)

$$i = j\tan\alpha\,\sin\theta \pm \left(\frac{\sin\theta}{\tan\phi} + \cos\theta\right)\sqrt{(1/4 - j^2)}. \tag{17}$$

This enables the imaged spots to be extracted via a HT which is 3-D in terms of the possible values for the center position along the epipolar line and the surface orientation angles ϕ and α. However, the nonlinear relationship of i in (17) with respect to ϕ and α severely limits the resolution of the HT accumulator array. For this reason it is preferable to use the HT formulated using (16) where i is linearly dependent on τ and γ. The surface orientation angles ϕ and α are then calculated for the peak values extracted from this HT accumulator array.

B. Color and Brightness Constraints to Restrict Voting

In practice, edge detection of the luminance image provides the edge points from which the HT arrays for each imaged spot are formed. Intuitive constraints are used to reduce the votes cast in the HT by edge points belonging to other spots. Color is used to resolve spatial ambiguity; each spot's position in the projected array may be identified from a codeword defined by the color of the spot and four of its neighbors. The coding scheme currently implemented is based upon that described by Griffin *et al*. [7]. Three spot colors are used: cyan, yellow, and magenta. Each image edge point is labeled as one of these colors by thresholding the mean image hue along a short line in the edge normal direction, which points toward the center of the spot. If an edge point has a different color to that of the desired spot, it is excluded from the HT voting process.

The imaged spot is brighter than the background so the normal direction of edge points for the desired spot should point toward the epipolar line, not away from it. If an edge point's gradient direction intersects with, or does not diverge from the direction of the epipolar line by an angle greater than $\pi/6$ rad, then it is included in the voting process. The inclusion of the divergence in the constraint introduces robustness to errors in the epipolar line position or the edge gradient direction. Applying this constraint reduces the number of votes cast in the array but does not affect the desired peak.

For the remaining voting edge points, the brightness provides an indication in which direction along the epipolar line the spot's center lies. Consider edge point A in Fig. 6, knowledge of which direction

(a) (b) (c)

Fig. 7. For part of a synthetic image of a planar surface: (a) the color image, (b) the edges plus an example epipolar line, and (c) the spot corresponding to the greatest HT peak.

is brightest implies that is where the spot lies. Let θ_+ and θ_- be the positive and negative depth directions of a line from A parallel to the epipolar line. Let θ_E be the edge gradient direction at point A, as measured via the edge detection operator. If $(\theta_+ + 2\pi/3)$ is greater than θ_E and $(\theta_+ - 2\pi/3)$ less than θ_E then votes are cast for the center position in the positive depth direction from the edge. If $(\theta_- + 2\pi/3)$ is greater than θ_E and $(\theta_- - 2\pi/3)$ less than θ_E then votes are cast for the center position in the negative depth direction from the edge. Edge points whose gradient direction is almost perpendicular to the direction of the epipolar line are able to vote in both directions to allow for the possible error in the epipolar line position and edge gradient. For the majority of edge points, application of this constraint casts a single plane of votes across the HT accumulator array instead of two.

V. Results

Results are presented which verify the new formulation of the HT and demonstrate how this new structured light system can be used to recover 3-D surface shape.

The scene is illuminated by a conventional 35 mm slide projector with slides created by a Laserwriter LRF. The 728×562 pixel images are captured in a 24 bit RGB format by a Sony XC711p color camera connected via a timebase corrector to a Quintek Mosaiq framestore. A simple luminance image is formed by taking the intensity of the brightest RGB component. The Canny edge operator is used here. A pin hole camera model is used for calibration of both the camera and projector, each represented by matrix transforming homogeneous coordinates [13].

The angle between projected and imaged rays is approximately 15°. The lenses used have long focal lengths to minimize perspective effects over the working volume. The imaged diameter of the spots, which does not change in the direction perpendicular to the epipolar line, is 23 pixels. The HT described here is for the application of capturing the 3-D shape of the face. The range chosen for the center positions along the epipolar line is equivalent to a variation in the 3-D surface location along the Z axis of the reference 3-D calibration coordinate of $30 \text{ mm} \leq Z \leq 90$ mm. The likely imaged spots' shapes are included within the ranges $0.3 \leq \gamma \leq 2.0$ and $-0.8 \leq \tau \leq 0.8$. The HT accumulator array is 3-D representing these parameter ranges by 209, 37, and 35 discrete levels, respectively, which is the finest resolution possible without peak spreading [4].

A. Spot Detection Via the HT

Fig. 7(a) shows part of a synthetic image for the 3-D planar surface $Z = 60$ mm calculated from the calibration data. Fig. 7(b) shows the corresponding edge image and the epipolar line for the expected center positions of one of the spots between $Z = 30$ mm and $Z = 90$ mm. The highlighted edge points are within the known spot size perpendicular to the epipolar line, and so are included in the formation of the HT accumulator array to extract the spot centered on the epipolar line. The spot with the parameters corresponding to the greatest peak in the HT accumulator array is drawn in Fig. 7(c), this is the correct spot centered on this epipolar line.

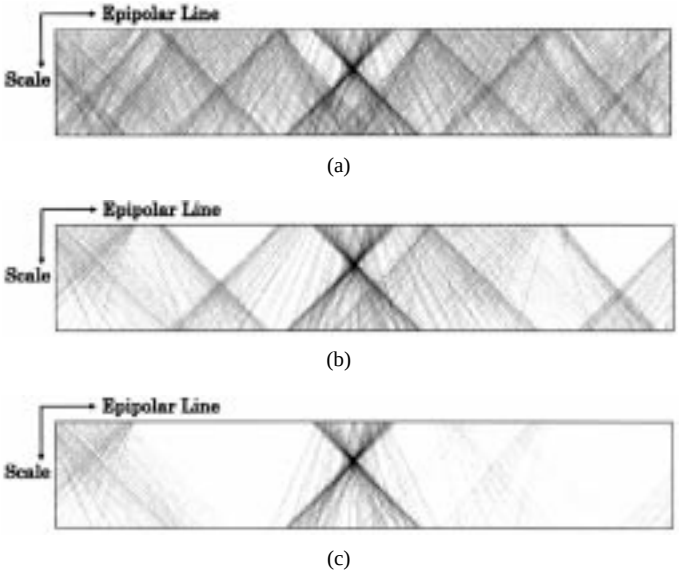

Fig. 8. Slices across the example HT accumulator array for the synthetic image (a) without voting constraints, total votes cast 723 919; (b) with only the color vote constraint, total votes cast 387 524; and (c) with both the color and brightness constraints, total votes cast 204 422.

Fig. 8 shows slices across three separate 3-D HT accumulator arrays, each with different voting constraints applied, formed to extract the spot centered on the epipolar line of Fig. 7(b). The two-dimensional slices across the 3-D HT accumulator arrays correspond to the shear at the maximum vote count. The darker areas of the HT slices indicate cells in the accumulator array which contain more votes. The linear way in which the votes are cast across the arrays is clearly visible. Fig. 8 demonstrates that the HT voting constraints greatly reduce the total number of votes cast in the accumulator array. For each of the three arrays of Fig. 8 the parameters of the greatest vote count and the greatest vote count itself are all identical. Thus the HT voting constraints are effective in reducing the total number of votes cast in the HT accumulator array without reducing the desired peak. This makes automatic peak extraction more robust.

B. The Structured Light System

This section presents results for a video-rate image sequence of a face during speech. To ensure that the projected colors were imaged

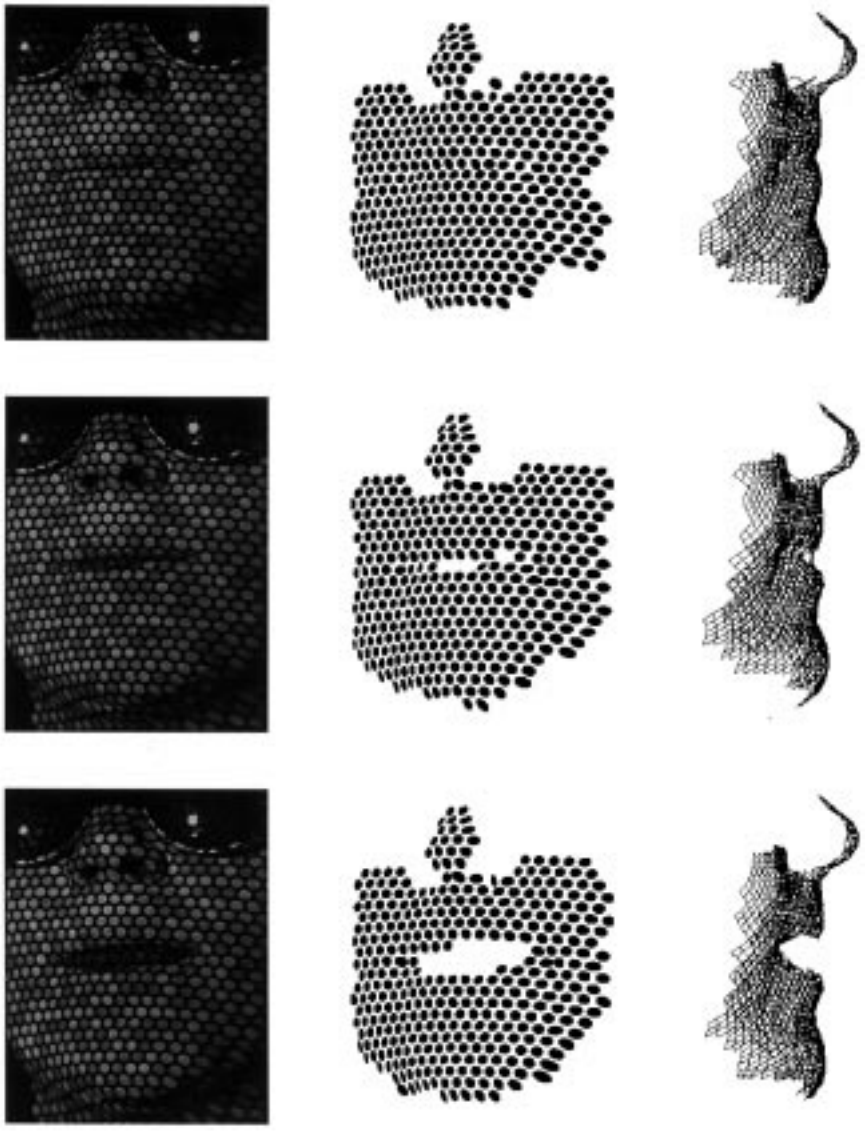

Fig. 9. Consecutive frames, extracted spots, and 3-D data for a video-rate speech sequence.

correctly, the face was painted white using theatrical makeup. Fig. 9 shows three consecutive frames, the extracted spots and 3-D data for the video-rate speech sequence. The HT provides several peaks of potential surface location and orientation for each spot in each frame. In general the greatest peak count is correct, but in some cases the epipolar line passes through the center of another spot of the same color which may produce a greater peak count. Thus a decoding algorithm is used to select the correct peaks for the spots. The algorithm is based upon simple constraints, for example no overlapping spots are allowed in the image. The decoding algorithm is not optimal but is sufficient to demonstrate that 3-D surface location and orientation may be extracted via color encoded spots. For display purposes the surface orientation data has been used to interpolate between the surface location samples in Fig. 9.

These results demonstrate that the location and orientation of 3-D surfaces may be captured via the new HT from a single image of a scene illuminated by the pattern of colored spots. Thus 3-D data may be collected for dynamic scenes at video rates.

VI. Conclusion

A structured light system based on a color encoded array of circular spots has been presented. Illuminating scenes with a single hexagonally tessellated array of colored spots enables video-rate surface data acquisition of moving objects.

A new formulation of the HT has been developed to extract 3-D surface location and orientation via each imaged spot. The 3-D surface location determines the position of each imaged spot's center along an epipolar line. The 3-D surface orientation determines the imaged shape of each spot. In the implementation of the HT, voting constraints based on color and brightness reduce greatly the number of votes cast in the accumulator array, and therefore the chance of a false peak arising, without reducing the desired peaks. Results verify both the new formulation of the HT and demonstrate the structured light sensor. Future work will investigate whether the partial spots created by surface step edges can be used to accurately locate and identify such surface features.

References

[1] P. J. Besl, "Active, optical range imaging sensors," in *Computer Vision: Principles*, R. Kasturi and R. C. Jain, Eds. New York: IEEE Comput. Soc. Press, 1991, pp. 36–61.

[2] K. L. Boyer and A. C. Kak, "Color-encoded structured light for rapid active ranging," *IEEE Trans. Pattern Anal. Machine Intell.*, vol. PAMI-9, no. 1, pp. 14–28, 1987.

[3] P. K. Commean, K. E. Smith, G. Bhatia, and M. W. Vannier, "Geometric design of a multisensor structured light range digitizer," *Opt. Eng.*, vol. 33, no. 4, pp. 1349–1358, 1994.
[4] C. J. Davies, "Three-dimensional sensing via colored spots," Ph.D. dissertation, Dept. Electron. Comput. Sci., Univ. Southampton, U.K., 1996.
[5] C. J. Davies and M. S. Nixon, "Feature extraction for video rate three dimensional imaging via colored spots," in *Canadian Conf. Electrical Computer Engineering*, 1995, vol. 2, pp. 916–919.
[6] S. M. Dunn, R. L. Keizer, and J. Yu, "Measuring the area and volume of the human body with structured light," *IEEE Trans. Syst., Man, Cybern.*, vol. 19, no. 6, pp. 1350–1364, 1989.
[7] P. M. Griffin, S. Lakshimi, and S. R. Yee, "Generation of uniquely encoded light patterns for range data acquisition," *Pattern Recognit.*, vol. 25, no. 6, pp. 609–616, 1992.
[8] R. M. Haralick and L. G. Shapiro, *Computer and Robot Vision: Vol. 1*. Reading, MA: Addison-Wesley, 1992.
[9] M. Ito and A. Ishii, "A three-level checkerboard pattern (TCP) projection method for curved surface measurement," *Pattern Recognit.*, vol. 28, no. 1, pp. 27–40, 1995.
[10] B. F. Jones and P. Plassmann, "An instrument to measure the dimension of skin wounds," *IEEE Trans. Biomed. Eng.*, vol. 42, no. 5, pp. 464–470, 1995.
[11] V. F. Leavers, *Shape Detection in Computer Vision Via the Hough Transform*. Berlin, Germany: Springer-Verlag, 1992.
[12] T. P. Monks and J. N. Carter, "Improved stripe matching for color encoded structured light," in *Lecture Notes in Computer Science 719*, D. Chetverikov and W. G. Kropatsch, Eds. Berlin, Germany: Springer-Verlag, 1993, pp. 466–485.
[13] I. E. Sutherland, "Three-dimensional data input by tablet," *Proc. IEEE*, vol. 62, no. 4, pp. 453–461, 1974.
[14] T. M. Van Veen and F. C. A. Groen, "Discretization errors in the Hough transform," *Pattern Recognit.*, vol. 14, pp. 137–145, 1981.
[15] P. Vuylsteke and A. Oosterlinckm, "Range image acquisition with a single binary-encoded light pattern," *IEEE Trans. Pattern Anal. Machine Intell.*, vol. 12, no. 2, pp. 148–164, 1990.
[16] S. R. Yee and P. M. Griffin, "Three-dimensional imaging system," *Opt. Eng.*, vol. 33, no. 6, pp. 2070–2075, 1994.

A Further Result on the Markov Chain Model of Genetic Algorithms and Its Application to a Simulated Annealing-Like Strategy

Joe Suzuki

***Abstract*— This paper shows a theoretical property on the Markov chain of genetic algorithms: the stationary distribution focuses on the uniform population with the optimal solution as mutation and crossover probabilities go to zero and some selective pressure defined in this paper goes to infinity. Moreover, as a result, a sufficient condition for ergodicity is derived when a simulated annealing-like strategy is considered. Additionally, the uniform crossover counterpart of the Vose–Liepins formula is derived using the Markov chain model.**

***Index Terms*—Genetic algorithms, Markov chain, simulated annealing.**

NOMENCLATURE

γ	Number of possible values which each gene takes.
$G = \{0, 1, \ldots, \gamma - 1\}$	Set of possible values which each gene takes.
L	Number of genes contained in each individual.
$N = \gamma^L$	Number of possible individuals.
$J = \{0, 1, \ldots, N-1\}$	Set of individuals.
$i_l, l = 1, 2, \ldots, N$	Individual with the lth largest fitness value.
$g[j] \in G, j = 0, 1, \ldots, L-1$	Value of the jth gene.
$i \in J$	individual (represented as both the string $g[0]\, g[1] \cdots g[L-1]$ and the integer $0 \le \sum_{j=0}^{L-1} \gamma^j g[L-1-j] \le N-1$).
$f(i), i \in J$	Fitness value of an individual i.
μ	Mutation probability.
χ	Crossover probability.
$F = \max\{f(i_{j+1})/f(i_j) : f(i_{j+1}) \neq f(i_j), 1 \le j \le N-1\}$	Fitness ratio.
$p = (\mu, \chi, F)$	Fixed parameters.
M	Number of individuals contained in each population.
0^+	Arbitrarily small positive value.
$\det A$	Determinant of a matrix A.
$\lvert S \rvert$	Cardinality of a set S.
$\delta(E)$	1 (if E is true), 0 (otherwise).
$H(i, i'), i, i' \in J$	Hamming distance between two individuals i and i'.
$\lvert i \rvert, i \in J$	Number of ones in an individual i.
$i \otimes i', i, i' \in J$	Bitwise multiplication of two individuals i and i'.
$i \oplus i', i, i' \in J$	Bitwise exclusive-or of two individuals i and i'.
$\bar{i}, i \in J$	One's complement of an individual i.
$\mu(t), t = 1, 2, \ldots$	Mutation probability of a generation t.
$\chi(t), t = 1, 2, \ldots$	Crossover probability of a generation t.
$m(t)$	Nondecreasing function of each generation t.
$F(t) = F^{m(t)}, t = 1, 2, \ldots$	$m(t)$ power of F.
$p(t) = (\mu(t), \chi(t), F(t))$	Valuable parameters.

I. INTRODUCTION

Genetic algorithms (GA's) are stochastic search techniques widely applied to combinatorial optimization problems [11], [14], [29], [30], [31], [32], [33]. GA's move from population to population. Each population consists of chromosomes (individuals) which represent candidate solutions to the optimization problem. A new population is formed by transforming individuals of the current population using stochastic operators (genetic operators) that emulate evolution in biological systems.

Our discussion is based on Davis's work [4], [5] on a simulated annealing (SA)-like strategy for simple GA's [11] in which a rigorous theoretical basis was constructed in addition to some empirical experiments. As usual, the following three basic genetic operations are applied to each generation change: selection, mutation, and crossover. However, intuitively, a wide space of solutions should be

Manuscript received September 4, 1995; revised July 26, 1996 and December 31, 1996.

The author is with the Department of Mathematics, Faculty of Science, Osaka University, Osaka, Japan (e-mail: suzuki@math.sci.osaka-u.ac.jp).

Publisher Item Identifier S 1083-4419(98)00209-X.